Verification of the Wavelet Adaptive Multiresolution Representation Method to a Prescribed Error Threshold

Steven Brill

Department of Aerospace and Mechanical Engineering

University of Notre Dame

Prepared for: AME 48491 Undergraduate Research

Advisors: Dr. Joseph M. Powers, Dr. Samuel Paolucci, Temistocle Grenga

June 4, 2014

Abstract

The Wavelet Adaptive Multiresolution Representation (WAMR) method numerically solves engineering problems based on partial differential equations to a user-prescribed level of accuracy. Moreover, it guarantees that the solution will have error of the same order of magnitude as the threshold. The method was verified for four different hydrodynamic shock problems that are commonly used for code verification. The results show that the error for a problem will always be less than the user-prescribed error threshold as expected. The WAMR method also produces a compressed image because the method uses an adaptive grid that only approximates the function in detail where necessary.

Contents

1 Introduction

A goal of many computational methods is to predict results observed in nature. The Wavelet Adaptive Mutliresolution Representation (WAMR) method is a computational method of solving problems that guarantees error less than a user-prescribed error, which is advantageous because many other methods only provide increased accuracy with a finer grid. As with any method, it must be verified so that it may be trusted on new problems. As Roache said [1], "The identification, elimination, and engineering 'proof' or demonstration of the absence of coding errors are the concern of Code Verification." Verification is a concept that is commonly confused with validation. Validation is solving the correct mathematical model, while verification is solving the mathematical model correctly. This study is only concerned with verification. In order to accurately verify the WAMR method, it was used to solve many test cases with accurate reference solutions. The test problems used are benchmark problems from the Enhanced Verification Test Suite (EVTS) [2] that are commonly used for verification of simulation codes. The goal of this verification is to allow the WAMR method to be used predictively and in cases where producing a solution to an automatically verified amount of error is advantageous. Unlike most codes, the evaluation of the WAMR method's success is not on decreasing error as the grid is refined. Instead, the method's success is measured by whether the solution meets the user-prescribed error criteria. These test problems will show that the WAMR method does guarantee that the solution meets a user-prescribed error; hence, the solutions are automatically verified.

The problems selected from the EVTS were selected because they each present different challenges for numerical codes. In general, the problems solved are multi-scale hydrodynamics problems. It is particularly important to find effective methods to solve multi-scale problems because they are computationally expensive [3]. The WAMR method is particularly useful for solving multi-scale problems because it provides an automatically verified solution, so once the problem is solved, no more effort will be necessary to verify the solution. The problems solved in this report all have analytical solutions or well-verified numerical solutions, so that the error of the solution from the WAMR method can be quantitatively verified.

2 Mathematical Model

The problems modeled are from hydrodynamics. More specifically, they are shock hydrodynamics problems with solutions that are the weak solutions of partial differential equations. In the EVTS the problems are modeled by the compressible Euler equations. However, the WAMR method cannot solve problems with embedded mathematical discontinuities, so viscosity and heat conduction terms were introduced into the model. In reality, the Euler equations are non-physical because there will always be diffusion at a sufficiently

small scale. Hence the WAMR method solves more physically relevant problems than the problems listed in the EVTS. Since the method is effective for multidimensional and multi-species problems, the general form of the Navier-Stokes equations solved for the problems are

$$\frac{\partial \rho}{\partial t} = -\frac{\partial}{\partial x_i}(\rho u_i) \tag{1}$$

$$\frac{\partial \rho u_i}{\partial t} = -\frac{\partial}{\partial x_j}(\rho u_j u_i + p\delta_{ij}) + \frac{\partial \tau_{ij}}{\partial x_j} \tag{2}$$

$$\frac{\partial \rho E}{\partial t} = -\frac{\partial}{\partial x_j}(u_j(\rho E + p)) + \frac{\partial}{\partial x_i}(u_j \tau_{ji} - q_i) \tag{3}$$

$$\frac{\partial \rho Y_k}{\partial t} = -\frac{\partial}{\partial x_i}(u_i \rho Y_k) - \frac{\partial j_{ik}}{\partial x_i}, \qquad k = 1, \ldots, K-1, \tag{4}$$

where t is the time, x_i is the position in the i direction, ρ is the density, u_i is the component of the velocity vector in the i direction, p is the pressure, δ_{ij} is the Kronecker delta, τ_{ij} is the viscous stress tensor for the i face and in the j direction, E is the specific total energy, q_i is the heat flux component in the i direction, Y_k is the mass fraction of species k, j_{ik} is the species mass flux of species k in the i direction, and M_k is the molecular mass of species k. The problems model ideal mixtures of calorically perfect ideal gas which are Newtonian fluids satisfying Fick's law and Fourier's law, so the constitutive relations are

$$\tau_{ij} = \mu\left(\frac{\partial u_i}{\partial x_j} + \frac{\partial u_j}{\partial x_i}\right) + \left(\kappa - \frac{2}{3}\mu\right)\frac{\partial u_l}{\partial x_l}\delta_{ij} \tag{5}$$

$$q_i = -\lambda\frac{\partial T}{\partial x_i} + \sum_{k=1}^{K}\left(h_k j_{ik} - \frac{RT}{M_k X_k} D_k^T d_{ik}\right) \tag{6}$$

$$j_{ik} = \frac{\rho Y_k}{\overline{M} X_k}\sum_{\substack{j=1 \\ j\neq k}}^{K} M_j D_{kj} d_{ij} - \frac{D_k^T}{T}\frac{\partial T}{\partial x_i} \tag{7}$$

$$d_{ik} = \frac{\partial X_k}{\partial x_i} + (X_k - Y_k)\frac{1}{p}\frac{\partial p}{\partial x_i} \tag{8}$$

$$e = c_v T + e_0 \tag{9}$$

$$E = e + \frac{1}{2}u_i u_i \tag{10}$$

$$p = \frac{\rho R T}{\overline{M}} \tag{11}$$

$$\sum_{k=1}^{K} Y_k = 1, \tag{12}$$

where μ is the shear mixture viscosity, κ is the bulk mixture viscosity, λ is the mixture thermal conductivity, T is the absolute mixture temperature, h_k is the enthalpy of species k, R is the universal gas constant, X_k is the mole fraction of species k, D_k^T are the thermal diffusion coefficients, d_{ik} is the mixture diffusion driving

force of species k in the i direction, $\overline{M}$ is the mixture molecular mass as defined in Appendix A, D_{kj} are the ordinary multicomponent diffusion coefficients, e is the mixture specific internal energy, c_v is the mixture specific heat at constant volume, and e_0 is the initial mixture specific internal energy.

The governing equations can be simplified in the one-dimensional, single species case. In the simplified case Eq. (1) becomes the same equation with $i = 1$. In the one-dimensional case $\delta_{ij} = 1$, $i = 1$, and $j = 1$ in Eq. (2) and Eq. (3). Eq. (4) is unnecessary with one component. The values of $j_{i,k}$ and $d_{i,k}$ are 0 in the single component case, so many terms from Eq. (5) and Eq. (6) can be removed along with the subscripts. Eq. (7), Eq. (8), and Eq. (12) become unnecessary when the problem is simplified. Eq. (9) remains unchanged. Eq. (10) has $i = 1$ and Eq. (12) can use the mass of the single species for $\overline{M}$. Also, since the gases are assumed to be calorically perfect ideal gases

$$e = c_v T, \tag{13}$$

$$\gamma = 1 + \frac{R}{c_v}, \tag{14}$$

$$\gamma = \frac{c_p}{c_v}, \tag{15}$$

where c_v is the specific heat of the mixture at constant volume, γ is the ratio of specific heats, and c_p is the specific heat of the mixture at constant pressure. Hence, the governing equations become much simpler in the one-dimensional, one species case. The problems are described dimensionally in the EVTS, so they were solved dimensionally in order to verify the WAMR method using the same method from the EVTS. However, the one-dimensional, single species Navier-Stokes equations were non-dimensionalized in Appendix B. The WAMR method can also solve the non-dimensionalized equations. One advantage of solving the non-dimensional equations is that solving the problem once would verify infinitely many other problems. Also, the EVTS unfortunately is restricted to problems with artificially low temperatures. With the non-dimensional equations one could solve a physical problem with the same solution as the non-physical problem in the EVTS. However, in order to verify the WAMR method according to the EVTS, the problems were solved dimensionally.

The EVTS initially models the shock as a perfect jump using the Heaviside step function. Once viscosity is introduced into the model, it is impossible to model the shock with the Heaviside step function. Instead, shocks were initially modeled using hyperbolic tangents as shown. This approximation also makes the model more physical than the model in the EVTS, because step functions do not occur in nature. An example of

a function used to initially model the pressure in a one-dimensional shock is

$$p = \frac{1}{2}\left[(p_H + p_L) - (p_H - p_L)\tanh\left(\frac{x - x_0}{\delta}\right)\right], \tag{16}$$

where p_H is the high pressure, p_L is the low pressure, x is the position, x_0 is the position of the shock, and δ is the thickness of the shock. For each problem δ is chosen to be small relative to the domain in order to most closely resemble the Heaviside step function.

The specific conditions for each problem will be explained later. The Sod problem, Shu-Osher problem, and Woodward-Colella problem all model one-dimensional, single species shocks, while the Richtmyer-Meshkov instability problem has multiple species and was solved in two-dimensions. The Sod problem models a shock caused by a jump in pressure [4]. The Shu-Osher problem models a shock with a sinusoidally varying pre-shock density [5]. The Woodward-Colella problem models the interactions of two shocks caused by two jumps in pressure [6]. The Richtmyer-Meshkov instability problem models a shock wave passing through a gas curtain in two dimensions [7].

3 Method

The WAMR method provides an accurate solution that meets a user-prescribed error value, ε. The method uses wavelets and scaling functions to form a multiscale basis. The first scaling function represents the function at the coarsest level. Then each of the following wavelets provide finer representations of the function. The wavelet amplitudes are the difference between the actual function value at a point and the value interpolated from the next coarsest grid. Hence the wavelet amplitudes provide a measure for the local approximation error at each collocation point. Then wavelets with amplitudes smaller than the user-prescribed error threshold are discarded. This method allows the WAMR method to limit the number of basis vectors while also guaranteeing that the solution meets the user-prescribed error. Representing a state variable $u(\mathbf{x})$ as a basis of wavelets with a threshold parameter, ε is given by the equation:

$$u^J(\mathbf{x}) = \underbrace{\sum_{\mathbf{k}} u_{0,\mathbf{k}}\Phi_{0,\mathbf{k}}(\mathbf{x}) + \sum_{j=0}^{J-1}\sum_{\{\boldsymbol{\lambda}\,:\,|d_{j,\boldsymbol{\lambda}}|\geq\varepsilon\}} d_{j,\boldsymbol{\lambda}}\Psi_{j,\boldsymbol{\lambda}}(\mathbf{x})}_{u_\varepsilon^J} \quad \underbrace{+\sum_{j=0}^{J-1}\sum_{\{\boldsymbol{\lambda}\,:\,|d_{j,\boldsymbol{\lambda}}|<\varepsilon\}} d_{j,\boldsymbol{\lambda}}\Psi_{j,\boldsymbol{\lambda}}(\mathbf{x})}_{R_\varepsilon^J},$$

where u_ε^J represents the wavelets with amplitude greater than the threshold and R_ε^J represents the wavelets with amplitude less than the threshold. Then the R_ε^J term is discarded in order to make a sparse grid. Figures 1 and 2 show an example function and the wavelet representation of the function [8]. These plots

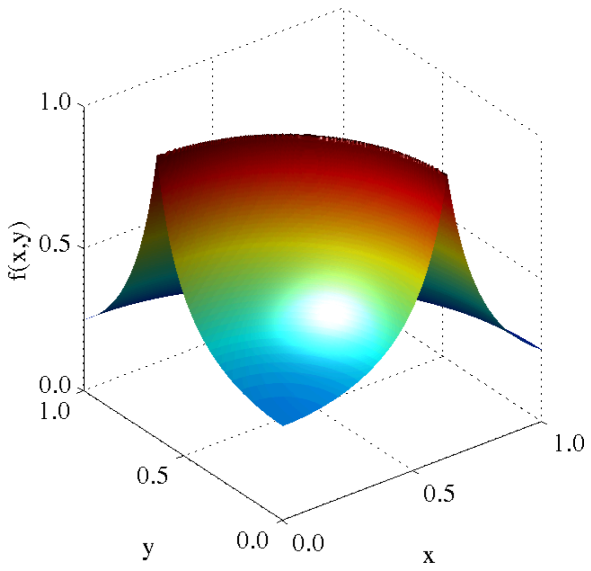

Figure 1: Example function $f(x, y) = 0.2/(|0.4 - x^2 - y^2| + 0.2)$

show how the WAMR method limits the number of necessary points by only putting the finest grid on a small portion of the domain. The WAMR method is also able to limit the time discretization error by using the smallest time step throughout the entire domain. The WAMR method adapts the grid with respect to space based on the details of the problem, which reduces the computation time necessary without affecting the detail of the solution. The test cases in this report will demonstrate that the WAMR method produces verified results based on the user-prescribed error criteria [8].

Since the goal is to show that the WAMR method is automatically verified, the error of the method must be evaluated. The solution for every parameter in the problem will have less error than that threshold. When an analytical solution is available, the error would be evaluated using the analytical solution, but for many problems there is no analytical solution. In those cases a reference solution was calculated using a finer grid than the grid created by the highest wavelet level of any of the solutions. The reference solutions were created by solving the problem using the same method, but with a very fine uniform grid instead of using the wavelet interpolation. Since the reference solution is created using a grid finer than any portion of the grid of the other solutions, the reference solution is guaranteed to be more accurate than the other solutions. Once an analytical or reference solution was found or created, the error was evaluated at every point on the grid for a specific variable at a fixed time. Then the maximum error was taken for each variable to verify that it was less than the user-prescribed error. The error formula is

$$error = \left\| \frac{U_n - U_a}{U_a} \right\|_\infty , \tag{17}$$

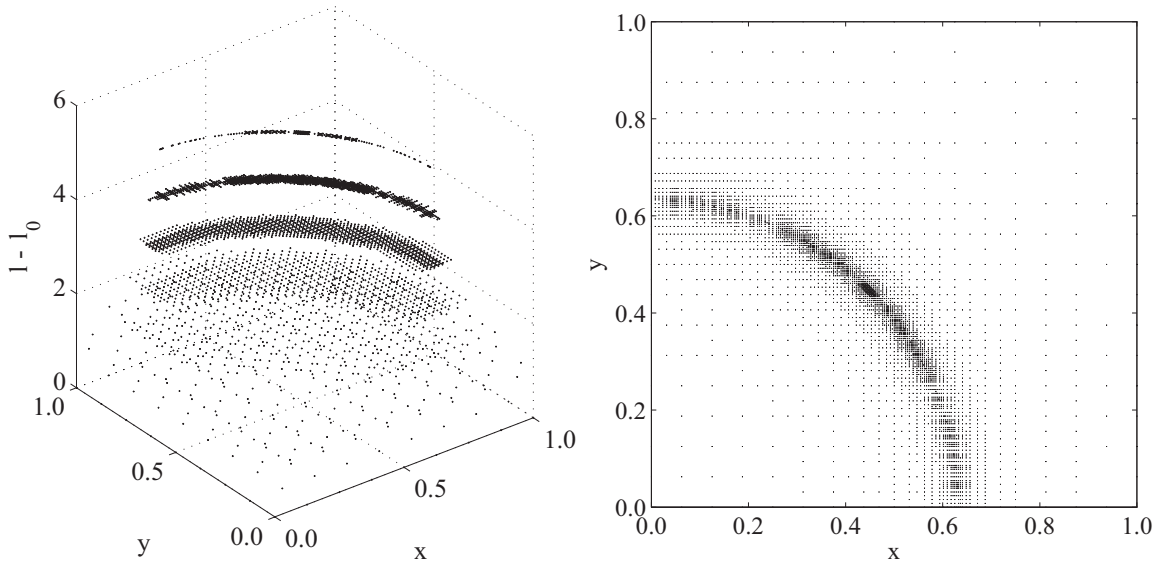

Figure 2: Collocation points of the example function for $\varepsilon = 5 \times 10^{-3}$

where U_n is the calculated solution value of field variable U and U_a is the actual value for field variable U. The error is evaluated at a fixed time at all points on the grid. Each problem was run for multiple ε values so that it could be confirmed that the error is automatically verified to be less than the user-prescribed error. The error for multiple different parameters was evaluated for each ε.

4 Results

Each of the problems was solved using multiple values of ε so that it can be verified that the error in the solution is automatically less than the used prescribed error threshold. Once the solutions for different ε values were complete, a reference solution was created using a uniform grid that is finer than the grid produced from the highest wavelet level of the other solutions. Then the error was evaluated based on the reference solutions. As the WAMR method solves the problem until a set final time, a set number of snapshots of the solution are saved in order to show that the method is correctly modeling all of the hydrodynamic interactions.

4.1 Sod Shock Tube Problem

The Sod shock tube problem is a problem modeled by the one-dimensional Euler equations. It is commonly used to verify computational hydrodynamics codes' abilities to handle hyperbolic equations. Initially two chambers of the gas are separated by an infinitely thin diaphragm. Each section of the chamber contains

different initial conditions. Many different sets of initial conditions can be used in the Sod problem, and the choice of initial conditions affects the computational challenges of the problem. For this verification two sets of initial conditions from the EVTS were used [4]. The problem could be physically modeled in a shock tube by removing a diaphragm or by puncturing a diaphragm with a plunger. Then the resulting shock could be observed.

Since the Sod problem is a one-dimensional, single species problem, the simplifications to the governing equations were used to solve the problem. The gas in the problem is a calorically perfect, ideal gas. The calorically perfect equation of state for an ideal gas is $p = (\gamma - 1)\rho e$ where γ is the ratio of specific heats. The problem statement assumed that the $\gamma = 7/5$ for the gas in use. In order to add viscosity to the inviscid problem defined in the EVTS, the gas was assumed to be diatomic nitrogen based on the given value of γ. However, the given parameters are so small that the initial temperature would be less than 1 K, which would mean the nitrogen is a liquid. Since gases are being modeled, the coefficient of viscosity and the coefficient of thermal expansion were assumed the be the coefficients for N_2 at 300 K instead of at the temperature prescribed in the problem. The coefficients were found to be $\mu = 1.813 \times 10^{-4}$ gm/(cm s) and $\lambda = 2618.7$ erg/(cm s K) using the CHEMKIN database. For this problem κ was taken to be 0. Since the problem contains a single shock, the shock was modeled in the same form as Eq. (16). For the Sod problems $\delta = 10^{-2}$ cm was chosen. For both sets of initial conditions the initial domain was divided into 100 grid points so that the initial grid accurately portrayed the solution while still allowing for the adaptive algorithm to efficiently display the solution.

Although the Sod problem as described in the EVTS has an analytical solution, that solution could not be used for error evaluation because the added viscosity makes it impossible to find an analytical solution. Instead, a reference solution was found by solving the problem using a fine grid. A fine grid of 102400 points was use to create the reference solution for each set of initial conditions.

4.1.1 Sod Problem 1

The first set of initial conditions is a simple test that is used to find problems resolving wave structure. There is an 8:1 density ratio and a 10:1 pressure ratio between the left and right sides of the shock. Initially, all of the gas starts at zero velocity. The problem is designed such that the ends of the tube do not affect motion of the shock.

The initial conditions were given in dimensional form in the EVTS [2], so the problem was solved dimensionally in order to verify the WAMR method using the method as stated in the EVTS. The dimensional initial conditions for the first Sod Problem are listed in Table 1 where x is the domain of the problem, x_i is the initial location of the shock, and t_f is the final time of the problem. The boundaries were prescribed

Table 1: Sod problem 1 initial conditions

	ρ [g/cm^3]	u [cm/s]	p [dyne/cm^2]
Left	1.0	0.0	1.0
Right	0.125	0.0	0.1
$0 \leq x \leq 1$ cm; $x_s = 0.5$ cm; $t_f = 0.25$ s			

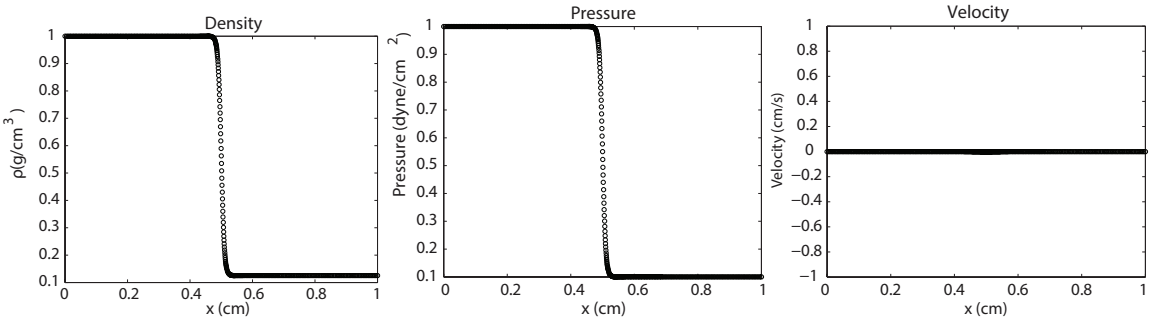

Figure 3: Sod problem 1 initial conditions

to maintain the initial conditions. The boundaries did not interact with the solution. In order to prevent boundary interaction the both boundaries were treated as zero stress boundaries.

For the first set of initial conditions, 10^3 solution snapshots were saved. A snapshot was taken every 250 μs. This problem was solved for $\varepsilon = 10^{-1}$, $\varepsilon = 10^{-2}$, $\varepsilon = 10^{-3}$, $\varepsilon = 10^{-4}$, $\varepsilon = 10^{-5}$, and $\varepsilon = 10^{-6}$. The maximum wavelet level used for the smallest ε was 6 so for the reference solution a 102400 point grid was used to ensure that the reference grid was finer than any of the grids from the WAMR method. The resolution scale level of the problem was 10. The size of the uniform grid was $\Delta x = 9.766 \times 10^{-6}$ cm. The initial conditions of the first Sod problem are plotted in Figure 3. There is a pressure and density drop across the shock, and all of the gas is initially at zero velocity.

The 500^{th} saved solution was recorded at $t = 0.125$ s. This solution accurately portrays the structure of a shock wave in Figure 4 for $\varepsilon = 10^{-6}$. At this time the shock has moved to $x = 0.715$ cm, and the contact discontinuity is visible around $x = 0.61$ cm. The rarefaction is visible to the left of the contact discontinuity. The initial conditions are preserved at both boundaries, and the boundaries do not affect the solution, which is as expected. There is a slight bump in the velocity graph around the location of the contact discontinuity. This bump would not exist in a physical or analytical solution. It is a result of assuming too large of a viscosity. Adding viscosity to the inviscid problem caused the sharp edges around the shock be become more smooth. However, the large assumed viscosity caused the contact to become smooth instead of a discontinuity as the name implies. The smoothness of the contact discontinuity also caused the bump on the velocity graph.

The final solution to the first Sod problem is shown in Figure 5. The form of shock in the final solution

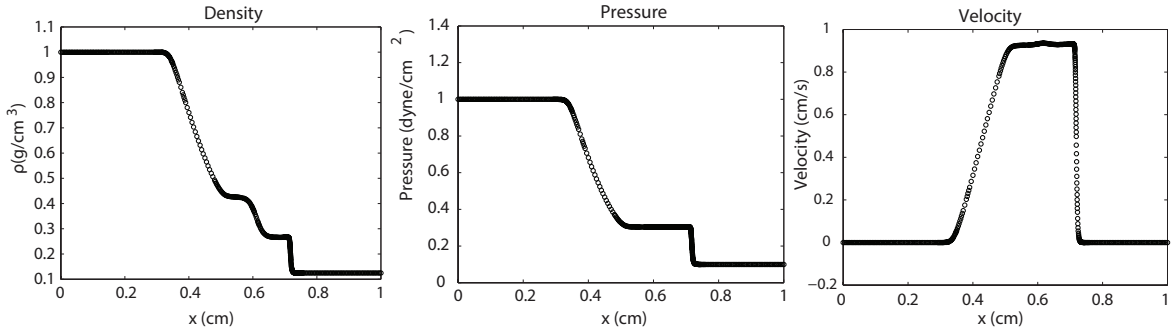

Figure 4: Sod problem 1 solution at $t = 0.125$ s

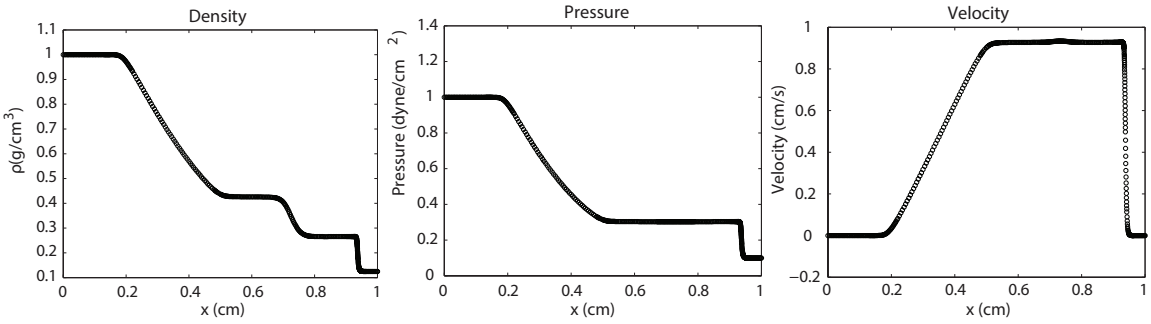

Figure 5: Sod problem 1 final solution

is similar to the solution in Figure 4. The shock has continued moving right and is now located around $x = 0.94$ cm. The contact discontinuity is also moving left and is located at $x = 0.74$ cm. It is also clear that the rarefaction is moving left as one would expect. The initial conditions are still preserved at the boundaries, and the boundaries have had no effect on the solution as prescribed in the problem definition.

Now the error must be evaluated for varying values of ε. The maximum error for pressure, density, and temperature at $t = 0.875 \times 10^{-2}$ s was plotted as a function of ε in Figure 6. Comparing the reference line with a slope of 1 to the error plots show that the maximum error for each variable as a function of ε has about a slope near 1. The graph of the error for the temperature intercepts the point $\left[10^{-4}, 4 \times 10^{-4}\right]$. Hence the measured error meets the prescribed error for each ε. Figure 7 shows that the error decreases as the resolution increases and that the resolution increases as ε decreases.

4.1.2 Sod Problem 2

The second Sod Problem has a transonic rarefaction wave. The problem has an 8:1 density ratio and a 10:1 pressure ratio between the left and right sides like the first problem. However, this problem has velocity on the left side of the shock and zero velocity on the right side. As with the first problem, the boundary does

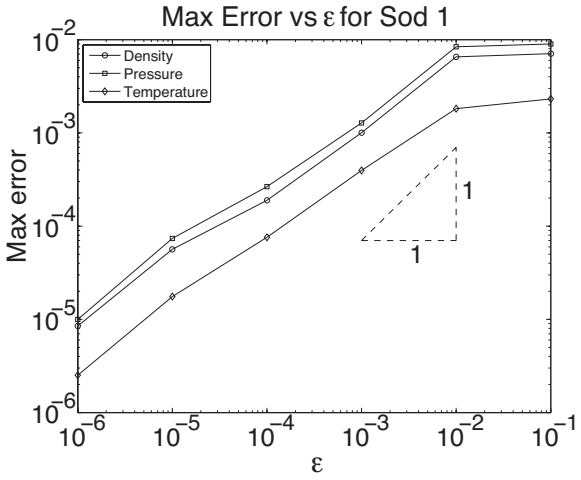

Figure 6: Sod 1 error vs ε at $t = 0.875 \times 10^{-2}$ s

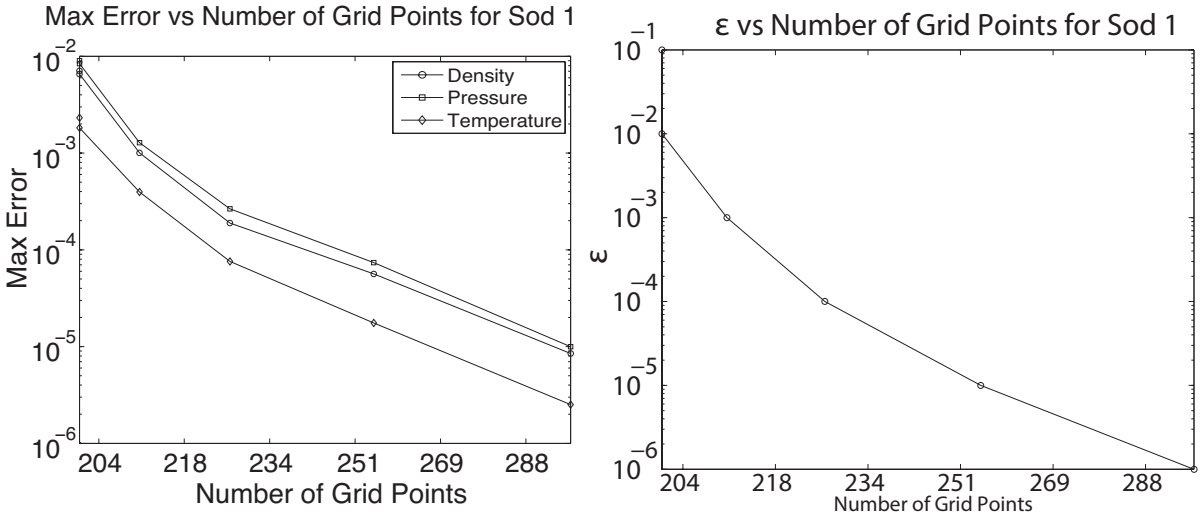

Figure 7: Sod 1 error vs ε at $t = 0.875 \times 10^{-2}$ s

Table 2: Sod problem 2 initial conditions

	ρ [g/cm^3]	u [cm/s]	p [dyne/cm^2]
Left	1.0	0.75	1.0
Right	0.125	0.0	0.1
$0 \leq x \leq 1$ cm; $x_s = 0.3$ cm; $t_f = 0.2$ s			

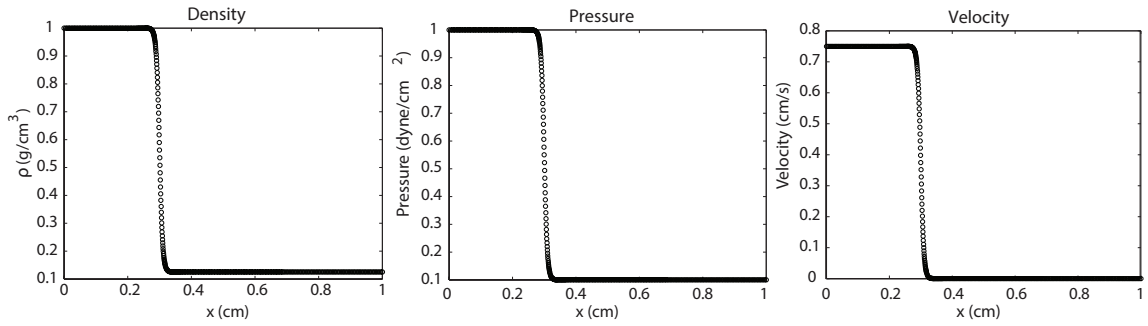

Figure 8: Sod problem 2 initial conditions

not affect the wave evolution.

The initial conditions for the second version of the Sod problem were also given dimensionally. The dimensional initial conditions for the second Sod Problem are listed in Table 2 where x is the domain of the problem, x_s is the initial location of the shock, and t_f is the final time of the problem. The boundaries were set to maintain the initial conditions and not to interfere with the solution. The left boundary was treated as an inflow boundary so that the velocity was always set to the initial velocity and the right boundary was a zero stress boundary.

For the second set of initial conditions, 10^3 solution snapshots were saved. A snapshot was taken every 200 μs. This problem was solved for $\varepsilon = 10^{-1}$, $\varepsilon = 10^{-2}$, $\varepsilon = 10^{-3}$, $\varepsilon = 10^{-4}$, $\varepsilon = 10^{-5}$, and $\varepsilon = 10^{-6}$. The maximum wavelet level for the smallest ε was 7 so for the reference solution a 102400 point grid was used to ensure that the reference grid was finer than any of the grids from the WAMR method. The resolution scale level of the problem was 10. The size of the uniform grid was $\Delta x = 9.766 \times 10^{-6}$ cm. The initial conditions of the second Sod problem are plotted in Figure 8. There is a pressure, density and velocity drop across the shock.

The 500^{th} saved solution was recorded at $t = 0.1$ s. This solution accurately portrays the structure of a shock wave in Figure 9 for $\varepsilon = 10^{-6}$. The solution portrays similar dynamics to the first Sod problem. At this time the shock has moved to $x = 0.51$ cm and the contact discontinuity is visible around $x = 0.43$ cm. The rarefaction is visible to the left of the contact discontinuity. The initial conditions are preserved at both boundaries are still preserved and the boundaries do not affect the solution, as expected. As with the first Sod problem, there is a slight bump in the velocity graph around the location of the contact discontinuity.

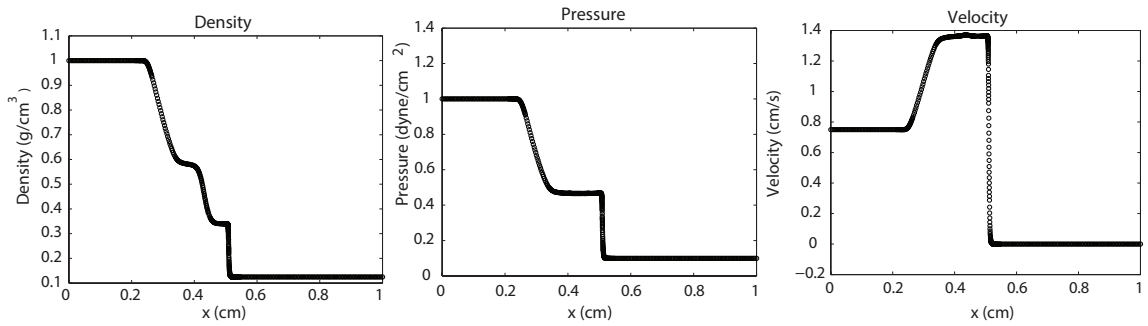

Figure 9: Sod problem 2 solution at $t = 0.1$ s

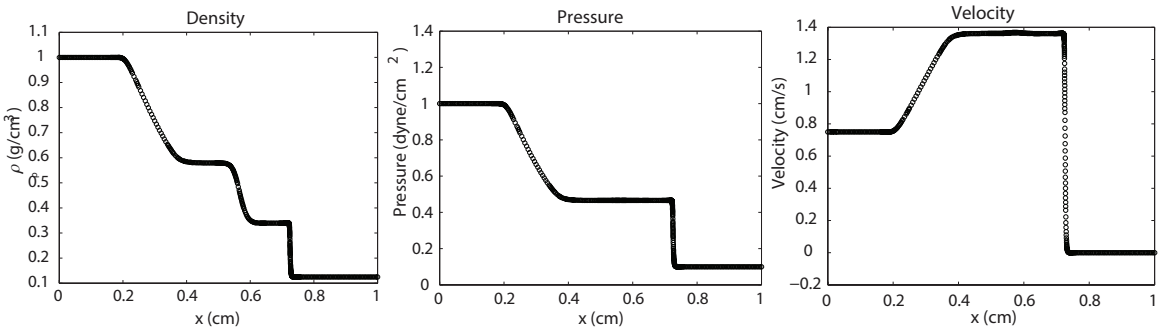

Figure 10: Sod problem 2 final solution

This is a result of assuming too much viscosity, like in the first problem.

The final solution to the second Sod problem is shown in Figure 10. The form of shock in the final solution is similar to the solution in Figure 9. The shock has continued moving right and is now located around $x = 0.725$ cm. The contact discontinuity is also moving left and is located at $x = 0.56$ cm. It is also clear that the rarefaction has moved left since the solution at the the halfway time. This shows that the rarefaction is able to travel through the gas, even though the gas has a velocity in the opposite direction. The boundaries did not affect the solution as prescribed by the EVTS.

The error from these solutions is the most important result. The error is plotted as a function of ε at $t = 0.26 \times 10^{-2}$ s in Figure 11. The error vs ε plot has a slope of about 1 and the temperature plot intercepts the point $\left[10^{-4}, 2 \times 10^{-5}\right]$. Hence the maximum error for each variable is below the error threshold. Figure 12 shows that the error decreases as the resolution increases and that the resolution increases as ε decreases.

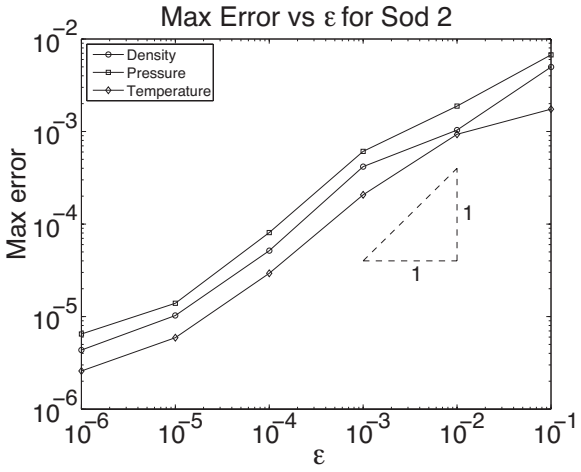

Figure 11: Sod 2 error vs ε at $t = 0.26 \times 10^{-2}$ s

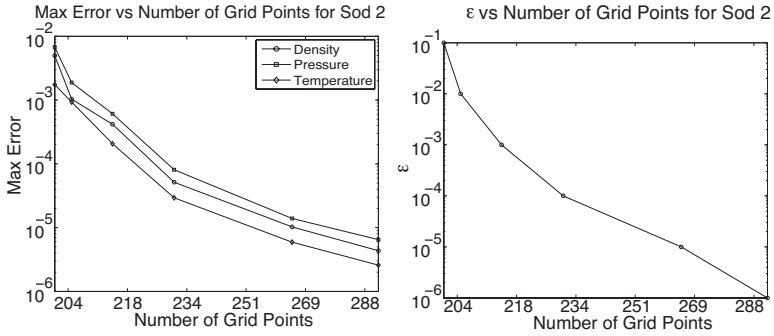

Figure 12: Sod 2 error vs ε at $t = 0.26 \times 10^{-2}$ s

Table 3: Shu-Osher problem initial conditions

	ρ [g/cm^3]	u [cm/s]	p [dyne/cm^2]
Left	3.857143	2.629369	10.33333
Right	1+ 0.2sin(5x)	0.0	1.0
$0 \leq x \leq 9$ cm; $x_s = 4.5$ cm; $t_f = 1.8$ s			

4.2 Shu-Osher Entropy Wave Problem

The Shu-Osher Entropy Wave Problem is a hydrodynamics problem used to test an algorithm's ability to handle complex flow structures in the presence of a shock wave. The problem also tests that a numerical method can handle fine scale flow structures and non-oscillatory solutions in the presence of shocks. The problem models a one-dimensional tube filled with an ideal gas with two sections separated by an infinitely thin diaphragm to simulate a Mach 5 shock. The post-shock conditions have a larger pressure and density and a velocity resulting from an inflow. The pre-shock conditions have zero velocity and a sinusoidally varying density. [5]

Since the Shu-Osher problem is a one-dimensional, single species problem, the simplifications to the governing equations were used to solve the problem. The same equation of state and gas were the same as in the Sod problem. The initial shock was modeled the same form as Eq. (16), but in this case the low pressure is a sinusoidally varying function. For the Shu-Osher problem $\delta = 10^{-2}$ cm was chosen. Similar to the Sod problem, the initial domain was divided into 100 grid points.

The initial conditions were given dimensionally in the EVTS [2] and are contained in Table 3 where x is the position, x_s is the initial location of the shock, and t_f is the final time of the problem. The initial velocity of the left side of the shock was originally calculated using the Rankine-Hugoniot jump conditions of the nominal pre-shock state. The left boundary condition is an inflow boundary condition that is always at the post-shock initial conditions. No boundary conditions were set on the right side, because the right side boundary is to be fixed at the pre-shock state, but the waves do not reach the right boundary when solving the problem. Hence, the lack of boundary conditions did not interfere with the solution.

For the Shu-Osher problem, 6×10^3 solutions were saved. A snapshot was take every 300 μs. The problem was solved for only $\varepsilon = 10^{-2}$, $\varepsilon = 10^{-3}$, and $\varepsilon = 10^{-4}$ because smaller ε values would be very computationally expensive, and larger ε causes errors in the code. Larger ε values create a grid with too few points so it does not capture the physics of the problem. Neither the inviscid nor viscous Shu-Osher problems have analytical solutions, so a fine grid reference solution was created. The maximum wavelet level used during the $\varepsilon = 10^{-4}$ solution was 13, so a grid of 6553600 points was used for the uniform grid. The resolution scale level of the problem was 16. The size of the uniform grid was $\Delta x = 1.373 \times 10^{-6}$ cm. The initial conditions contains a jump in pressure, velocity and density at the shock. Also, the density on the

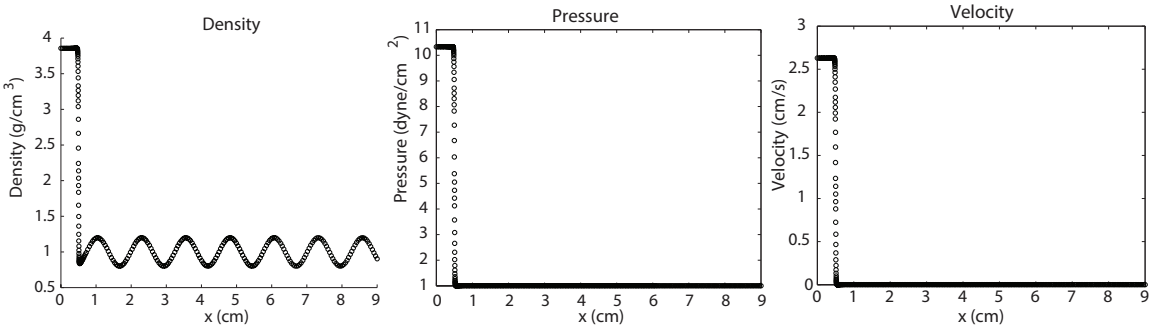

Figure 13: Shu-Osher problem initial conditions

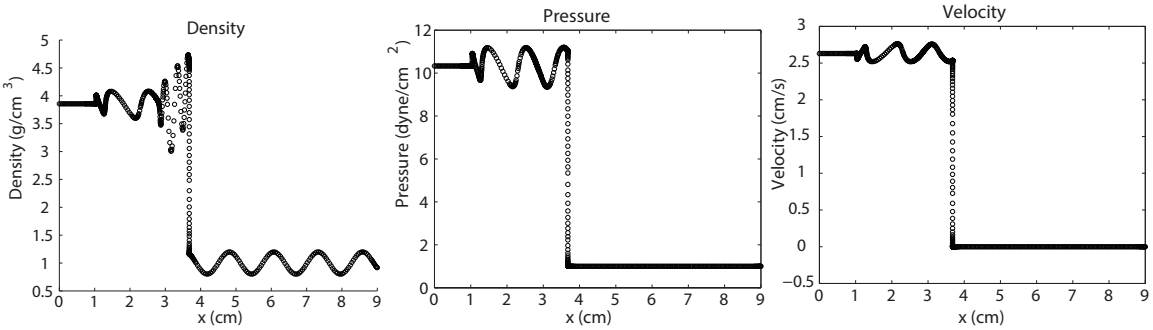

Figure 14: Shu-Osher problem at $t = 0.9$ s

right side of the shock varies sinusoidally as shown in Figure 13.

An intermediate solution at $t = 0.9$ s is shown for $\varepsilon = 10^{-4}$ in Figure 14. At this time the shock has moved to $x = 3.7$ cm. High amplitude and high velocity density waves follow the shock. However as the sinusoidal density gets further away from the shock, its amplitude and frequency decrease to a value similar to the initial pre-shock density profile. Also there is a contact discontinuity at $x = 1.05$ cm.

The final solution has a similar structure to the intermediate solution. Figure 15 shows a comparison between the final density profile as given in the EVTS and the final density results using the WAMR method for different ε values. The solution provided in the EVTS is the solution to the inviscid problem, so the solutions should not match perfectly. However the solutions are very similar, so it is clear that the added viscosity had little effect on the problem.

The error as a function of ε has about a slope of 1 as shown in Figure 16. Also note that the error from the solution for each variable has error less than the user-prescribed error threshold. Hence, the method is verified. Also, Figure 17 shows that for the Shu-Osher problem as the ε decreases, the number of points increase. As the number of points increases the error decreases as expected. Hence the solution is much more compact when using the WAMR method.

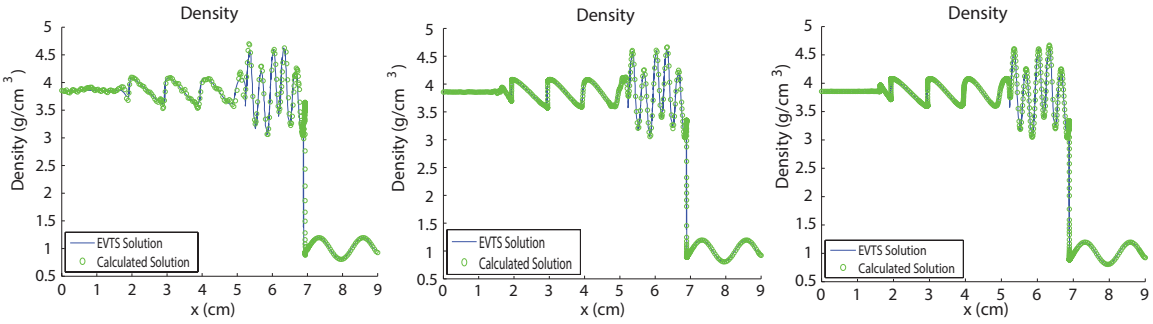

Figure 15: Shu-Osher solution vs. EVTS result

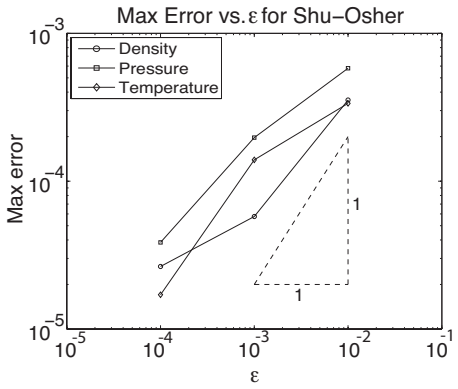

Figure 16: Shu-Osher error vs. ε at $t = 0.3 \times 10^{-3}$

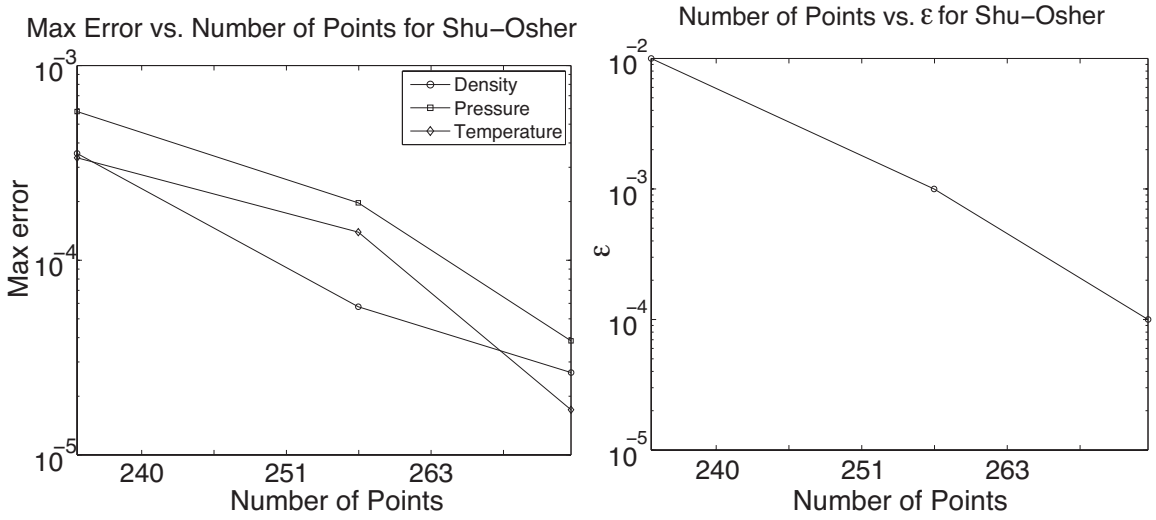

Figure 17: Shu-Osher grid size $t = 0.3 \times 10^{-3}$

4.3 Woodward-Colella Blast Wave Problem

The Woodward-Colella problem is a hydrodynamics problem that tests a method's ability to track contact surfaces, capture shocks, and handle strong shock interactions. It tests an algorithm's ability to numerically handle complex wave interactions and strong shocks. The Woodward-Colella problem models a one-dimensional tube filled with a calorically perfect ideal gas. The gas is separated into three sections with two infinitely thin diaphragms all with zero velocity and constant density. The left section takes up 10% of the tube and has the highest pressure. The middle section contains 80% of the tube and has the lowest pressure. The right section takes up 10% of the tube and has an intermediate pressure. The ends of the tube are sealed. Once the diaphragms are broken, two strong shocks approach the center causing complex wave interactions [6].

Like the first two problems, the Woodward-Colella problem could also be modeled in a shock tube. However, for this case, three regions of gas would need to be created using two diaphragms. The initial conditions in each chamber would be different and then the shock would begin when both diaphragms were removed or punctured with plungers.

Since the Woodward-Colella problem is a one-dimensional, single species problem, the simplifications to the governing equations were used to solve the problem. The same equation of state and gas assumptions as the Sod problem and the Shu-Osher problem were used for this problem. Since the Woodward-Colella problem contains two shocks, Eq. (16) will not apply for this problem. Instead, a different function was developed to contain two shocks. The initial pressure is described by the function

$$p = \frac{p_L}{4}\left[\left(1+\frac{p_M}{p_L}\right)-\left(1-\frac{p_M}{p_L}\right)\tanh\left(\frac{x-x_2}{\delta}\right)\right]\left[\left(\frac{p_H}{p_L}+1\right)-\left(\frac{p_H}{p_L}-1\right)\tanh\left(\frac{x-x_1}{\delta}\right)\right], \qquad (18)$$

where p_L is the low pressure, p_M is the medium pressure, p_H is the high pressure, x is the position, x_1 is the position of the first shock, x_2 is the position of the second shock, and δ is the thickness of the shock. The thickness of both shocks was set at $\delta = 10^{-3}$ cm in order to be sufficiently small relative to the domain. Also, the initial grid was divided into 100 grid points, like the first two problems.

The initial conditions were given dimensionally in the EVTS [2] and are contained in Table 4 where x is the position, x_1 is the initial location of the first diaphragm, x_2 is the initial location of the second diaphragm, and t_f is the final time of the problem. The left and right boundaries of the tube are both walls, so the boundary conditions of the problem set the velocity at both walls to be zero. No other boundary conditions were used to solve this problem.

For the Woodward-Colella Blast Wave problem, 100 solutions were saved. A snapshot was saved every 380 μs. As with the Shu-Osher problem, this problem was also solved for $\varepsilon = 10^{-2}$, $\varepsilon = 10^{-3}$, and $\varepsilon = 10^{-4}$,

Table 4: Woodward-Colella problem initial conditions

	ρ [g/cm^3]	u [cm/s]	p [dyne/cm^2]
Left	1.0	0.0	10^3
Middle	1.0	0.0	10^{-2}
Right	1.0	0.0	10^2
$0 \leq x \leq 1$ cm; $x_1 = 0.1$ cm; $x_2 = 0.9$ cm; $t_f = 0.038$ s			

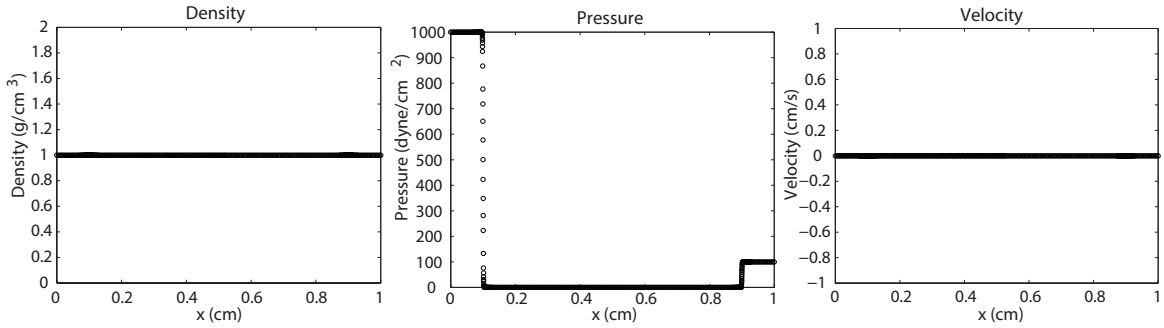

Figure 18: Woodward-Colella initial conditions

because smaller ε values would cause the problem to become much more computationally expensive. Neither the inviscid nor viscous Woodward-Colella problems have analytical solutions, so a fine grid reference solution was created. The maximum wavelet level used in the smallest ε solution was found to be 13 so a uniform grid of 6553600 points was used in order to make a uniform grid sufficiently finer than the solutions using the WAMR method. The resolution scale level of the problem was 16. The size of the uniform grid was $\Delta x = 1.526 \times 10^{-7}$ cm. This uniform grid was used to calculate the reference solution. The initial conditions plotted in Figure 18 show the two initial jumps in pressure.

The two shocks approach each other as seen in the plots at $t = 0.019$ s in Figure 19. Then the shocks hit each other causing complex interactions which are accurately modeled as shown in Figure 20 at the final time of $t = 0.038$ s. The EVTS included an image of density the final solution to the inviscid Woodward-Colella problem. When that solution is superimposed on the final solution using the WAMR method with an error threshold of $\varepsilon = 10^{-4}$, one can see that the result is very similar. Figure 21 shows that the WAMR solution is very similar to the inviscid solution, but they are slightly different around the corners and at the discontinuities. These differences were expected when viscosity was added to the problem.

The error for the Woodward-Colella problem will be reported at a later date, because the computational intricacies of the problem cause it to be computationally more expensive. It is currently in process and error will be reported as soon as a solution is saved. However, one should expect that the error will be less than the user-prescribed error criteria.

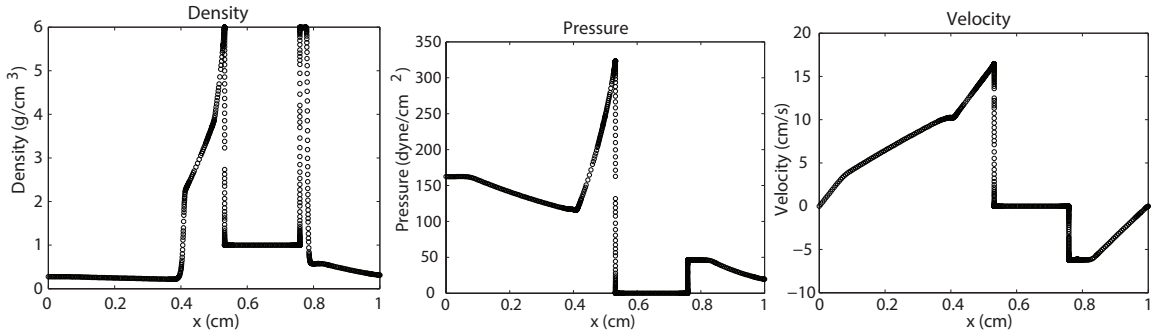

Figure 19: Woodward-Colella at $t = 0.019$ s

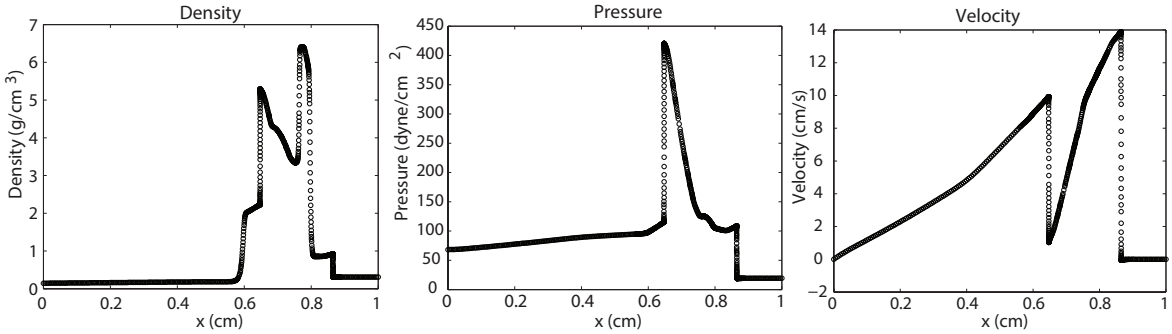

Figure 20: Woodward-Colella at $t = 0.038$ s

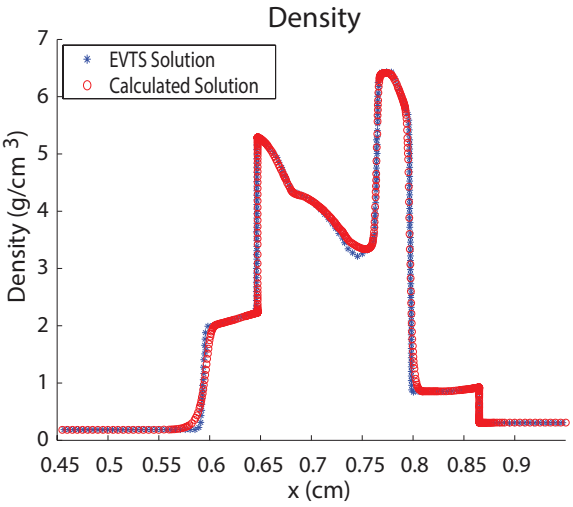

Figure 21: Woodward-Colella at $t = 0.038$ s compared to EVTS solution

4.4 Richtmyer-Meshkov Instability Problem

The Richtmyer-Meshkov Instability (RMI) problem is a hydrodynamics problem that is used to test how codes handle multiple fluid interactions in the presence of shocks. It also tests how a method captures large and fine scale dynamics of the mixing layer. The problem was modeled in two dimensions. In general, the problem discusses the stability of an accelerated interface separating two incompressible fluids. Initially a sinusoidal shaped gas curtain of SF_6 is at rest in a shock tube of air. Then a shock of high pressure air moves through gas curtain, which causes instability. Next, the shock bounces off the end of the tube and hits the initial instability causing complex instabilities to occur. The vortex dynamics of the RMI are detailed in other sources [9–11].

The Richtmyer-Meshkov problem can be tested in a shock tube, like the first four problems. The RMI is relevant many different situations in engineering; it is important in the mixing in ramjet engines [12,13]; it helps model the mixing in supernovæ [14,15]; it plays a key role in describing the deflagration-to-detonation transition [16].

The RMI problem is a two dimensional, multi-fluid problem so the general form of the governing equations were used to solve the problem. The quiescent fluids chosen for the problem were air for the main fluid and SF_6 for the gas curtain. For this problem, air mixture was defined as 23.2% mass O_2 and 76.8% mass N_2. The problem was designed to have a single mode sinusoidal perturbation at the interface between the gases. The gas curtain was described by

$$Y_{SF_6} = 10^{-12} + \frac{A\left(1 + B\cos\left(k\left(y - 0.18\text{cm}\right)\right)\right)}{1+B} e^{\frac{-2\alpha(x-x_o)^2}{(1+\beta\cos(k(y-0.18\text{cm})))^2}}, \tag{19}$$

where Y_{SF_6} is the mass fraction of SF_6, y is the position in the y direction, x is the position in the x direction, x_0 is the location of the gas curtain in the x direction, and A, B, k, α, and β are constant parameters defined in Table 5. The shock occurred in the air region and was defined in the same form at Eq (16) for pressure, temperature, and velocity. The initial conditions are described in Table 6 where a_L is the acoustic speed to the left of the shock, a_R is the acoustic speed to the right of the shock, t_s is the location of the shock in the x direction, and t_f is the final time. The shock thickness was defined to be $\delta = 10^{-4}$ cm so that δ is sufficiently small relative to the domain. The density is much higher in the gas curtain than in the surrounding error because the curtain is made of SF_6. All boundaries were set as zero stress boundaries. The left end of the tube allowed an inflow of air at the post shock conditions. On the left and right walls, the velocity is set to zero in the x direction and on the top and bottom walls the y directional velocity is zero.

For the Richtmyer-Meshkov instability problem, 250 solutions were saved. Each solution was saved every 2.5 μs. The problem was solved for $\varepsilon = 10^{-1}$, $\varepsilon = 10^{-2}$, and $\varepsilon = 10^{-3}$. Due to the large computation

Table 5: RMI problem gas curtain coefficients

A	B	k (rad/cm)	α	β
0.97	0.2	$2\pi/0.36$	8.36	-0.04
$0 \leq x \leq 15$ cm; $0 \leq y \leq 1.1$; $x_0 = 4.3$ cm				

Table 6: Richtmyer-Meshkov problem initial conditions

	p [dyne/cm^2]	T [K]	u [cm/s]
Left	1.202×10^6	338.4	$1.2a_L - 0.8422a_R$
Right	7.95×10^5	300.0	0.0
$0 \leq x \leq 15$ cm; $0 \leq y \leq 1.1$; $x_s = 3.0$ cm; $t_f = 6.25 \times 10^{-4}$ s			

time associated with this 2-dimensional problem there was no solution on a uniform grid. The initial gas curtain of SF_6 can be seen in Figure 22. Another solution at $t = 1.925 \times 10^{-4}$ s was recorded showing how the shock initially disturbs the gas curtain in Figure 23. Then the shock continues to hit the wall as shown in Figure 24.

The error could not be effectively computed because the saved solutions were created with a dynamic time-step. The dynamic time-step caused solutions to be saved at different times, so error could not be measured. Comparing two solutions at even slightly different time steps would make the solution appear to have a large amount of error, which may not be the case. However, the accuracy of the solutions can be seen in the detail of the solution. High magnification solutions of the RMI problem at $t = 1.925 \times 10^{-4}$ are shown in Figure 25 for $\varepsilon = 10^{-1}$, $\varepsilon = 10^{-2}$, and $\varepsilon = 10^{-3}$. As the the ε value gets smaller, the area of the high density becomes more defined and the general shape of the instability becomes more round. Hence the solutions with lower ε values are more accurate.

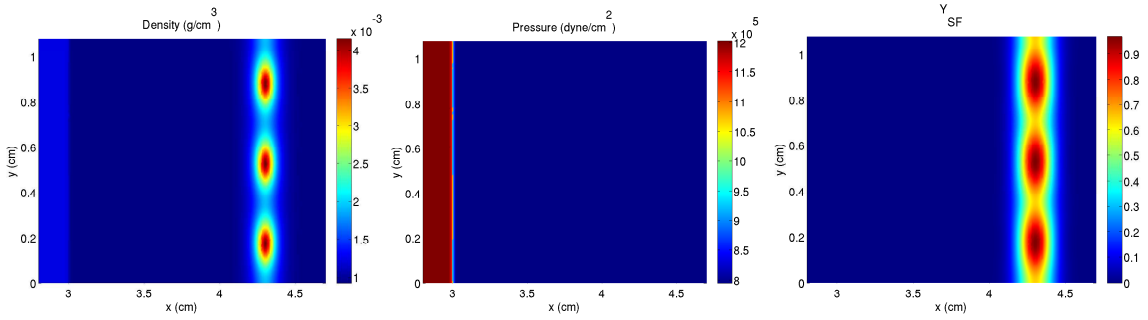

Figure 22: Richmyer-Meshkov initial conditions

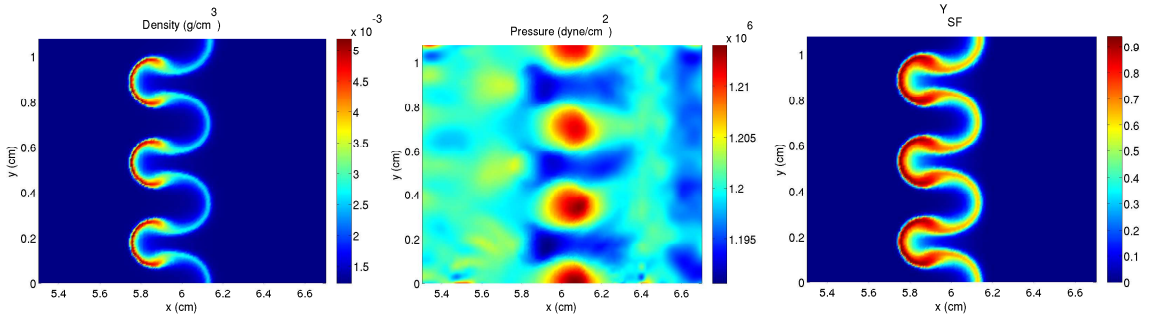

Figure 23: Richmyer-Meshkov at $t = 1.925 \times 10^{-4}$ s

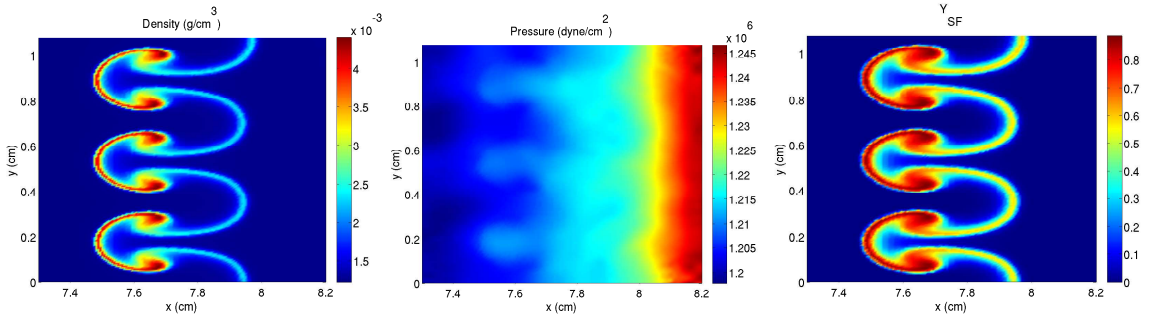

Figure 24: Richmyer-Meshkov at $t = 3.6 \times 10^{-4}$ s

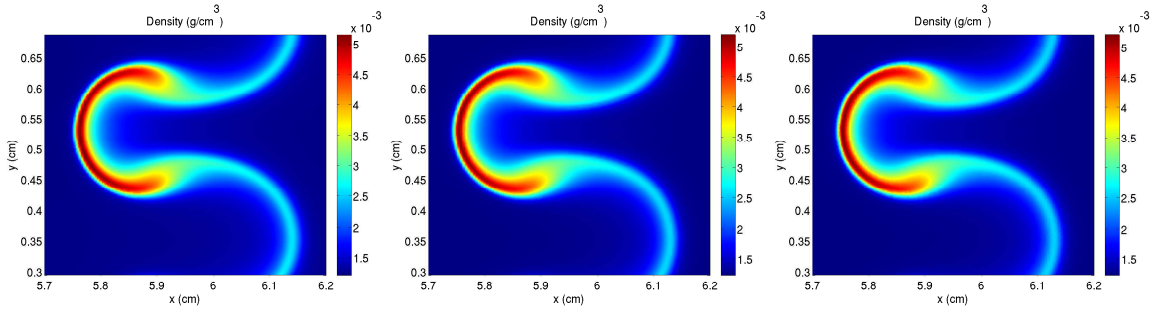

Figure 25: Richmyer-Meshkov detailed comparison

5 Discussion and Conclusions

The error from both Sod problems show that the error initially meets the user-prescribed error criteria, but over time the error gets worse. These results imply there is error introduced during the time discretization. The error introduced in time is a result of using too large of a time step. The time-step used for the second Sod problem was $\Delta t = 0.1 \times 10^{-7}$ s. In order to ensure the accuracy of a numerical solution with diffusion one must insist that $\Delta t \leq (\Delta x)^2 / (\mu/\rho)$. For the first Sod problem Δt should be much less than 5×10^{-8} s. Rerunning the problem with a lower time-step should eliminate most of the error introduced in time.

The slope of the error vs. ε plot should be 1 because for each ε the error should be of the same order of magnitude. For example, Figure 16 has about a slope of 1. However, Figure 16 also shows that the error is over an order of magnitude below the user-prescribed error. The WAMR method produced results with less error than prescribed because the initial grid fine enough that it eliminates some of the error allowed by the WAMR method. They show that while the WAMR method is guaranteed to meet the user-prescribed error, it can produce results that have less error than prescribed.

The error plots for each solution show that the WAMR method is verified. In each case it provides an error value that is less than the user-prescribed error. This is not just true for one ε but for a range of values. Hence the solution for any value of ε chosen by the user. Verification that the WAMR method shows that the method provids an automatically verified solution.

The problems were taken from the EVTS so that the WAMR method could be verified in the same manner as other computational codes, but diffusion was added to the problems in order to solve them with the WAMR method. The viscosity and the thickness of hyperbolic tangent functions was set low in order to reduce the impact of the modifications on the final solution. Figure 15 shows that modifications have little effect on solution. Figure 21 shows that the viscosity makes corners appear more round in the solution, but the overall shape of the solution is preserved. The approximations for viscosity and thermal conductivity were effective to maintain the shape of the solution, but they could be improved. Figure 5 shows that the contact discontinuity is too gentle and it is not a discontinuity. The viscosity also influences the velocity plot by causing a small bump to occur at the same location as the contact discontinuity. These issues can be mended by assuming a smaller coefficient of viscosity. Since the problem is at a very low temperature and pressure assuming a very small viscosity will not negatively affect the solution. Instead it will make the jumps more closely resemble the discontinuities in the inviscid problem.

The verification of the method implies that the WAMR method can be used to solve new problems to a set error criteria. Most other computational methods do not allow a user to set the error in advance, so the WAMR method has a unique advantage over other methods. The compression of the function with

the wavelets also provides advantages over other methods because it helps to solve the problem quickly. For example, the first Sod problem took about a day to run at $\varepsilon = 10^{-6}$ while the uniform grid without the wavelet interpolation was running for two weeks and still did not reach the final time. The compression created by the wavelets makes the WAMR method much less computationally expensive than other methods, like the uniform grid.

In conclusion, the WAMR method provides automatically verified results. Five problems from the EVTS were used to test the verification. The error from each solution met the user-prescribed error criteria. The WAMR method is unique because it produces an automatically verified solution and because it is computationally less expensive than other methods. The WAMR method produces a more compact grid for each problem which save computational time.

References

[1] P. J. Roache. *Fundamentals of verification and validation*. Hermosa, Sorroco, NM, 2009.

[2] J. R. Kamm, J. S. Brock, S. T. Brandon, D. L. Cotrell, B. Johnson, P. Knupp, W. J. Rider, T. G. Trucano, and V. G. Weirs. Enhanced verification test suite for physics simulation codes. *Los Alamos National Laboratory*, (SAND 2008-7813).

[3] T. J. Barth, T. Chan, and R. Haimes. *Multiscale and multiresolution methods: Theory and applications*, volume 20. Springer, 2002.

[4] G. A. Sod. A survey of several finite difference methods for systems of nonlinear hyperbolic conservation laws. *Journal of Computational Physics*, 27(1):1–31, 1978.

[5] C. Shu and S. Osher. *Efficient implementation of essentially non-oscillatory shock-capturing schemes, II*. Springer, Berlin, 1997.

[6] P. Woodward and P. Colella. The numerical simulation of two-dimensional fluid flow with strong shocks. *Journal of Computational Physics*, 54(1):115–173, 1984.

[7] R. D. Richtmyer. Taylor instability in shock acceleration of compressible fluids. *Communications on Pure and Applied Mathematics*, 13(2):297–319, 1960.

[8] S. Paolucci, Z. J. Zikoski, and D. Wirasaet. WAMR: An adaptive wavelet method for the simulation of compressible reacting flow. part i. accuracy and efficiency of algorithm. *Journal of Computational Physics*, accepted and in press, 2014.

[9] D. L. Cotrell and A. W. Cook. Scaling the incompressible Richtmyer-Meshkov instability. *Physics of Fluids*, 19(7):078105, 2007.

[10] D. Lee, G. Peng, and N. J. Zabusky. Circulation rate of change: A vortex approach for understanding accelerated inhomogeneous flows through intermediate times. *Physics of Fluids*, 18(9):097102, 2006.

[11] N. J. Zabusky. Vortex paradigm for accelerated inhomogeneous flows: Visiometrics for the Rayleigh-Taylor and Richtmyer-Meshkov environments. *Annual Review of Fluid Mechanics*, 31(1):495–536, 1999.

[12] E. T. Curran, W. H. Heiser, and D. T. Pratt. Fluid phenomena in scramjet combustion systems. *Annual Review of Fluid Mechanics*, 28(1):323–360, 1996.

[13] J. Yang, T. Kubota, and E. E. Zukoski. Applications of shock-induced mixing to supersonic combustion. *AIAA Journal*, 31(5):854–862, 1993.

[14] W. D. Arnett, J. N. Bahcall, R. P. Kirshner, and S. E. Woosley. Supernova 1987a. *Annual Review of Astronomy and Astrophysics*, 27:629–700, 1989.

[15] A. Burrows, J. Hayes, and B. Fryxell. On the nature of core collapse supernova explosions. *Astrophysics Journal*, 450:830–850, 1995.

[16] A. M. Khokhlov, E. S. Oran, and G. O. Thomas. Numerical simulation of deflagration-to-detonation transition: the role of shock–flame interactions in turbulent flames. *Combustion and Flame*, 117(1):323–339, 1999.

6 Appendix A

The definition of mixture molecular mass is

$$\overline{M} = \sum_{k=1}^{K} Y_k m_k \tag{20}$$

where $\overline{M}$ is the mixture molecular mass, Y_k is the mass fraction of species k, and m_k is the molecular mass of species k.

7 Appendix B

This appendix will detail the non-dimensionalization of the one-dimensional compressible Navier-Stokes equations. The equations before non-dimensionalization are:

$$\frac{\partial \rho}{\partial t} + \frac{\partial}{\partial x}(\rho u) = 0, \tag{21}$$

$$\frac{\partial}{\partial t}(\rho u) + \frac{\partial}{\partial x}(\rho u^2 + p - \tau) = 0, \tag{22}$$

$$\frac{\partial}{\partial t}\left(\rho\left(e + \frac{u^2}{2}\right)\right) + \frac{\partial}{\partial x}\left(\rho u\left(e + \frac{u^2}{2}\right) + u(p - \tau) + J^q\right) = 0, \tag{23}$$

$$\tau = \frac{4}{3}\mu\frac{\partial u}{\partial x}, \tag{24}$$

$$J^q = -\kappa\frac{\partial T}{\partial x}, \tag{25}$$

$$p = \rho R T, \tag{26}$$

$$e = c_v T, \tag{27}$$

$$\gamma = 1 + \frac{R}{c_v} \tag{28}$$

The definitions for nondimensional quantities are as follows:

$$\tilde{\rho} = \frac{\rho}{\rho_0}, \tag{29}$$

$$\tilde{P} = \frac{P}{P_0}, \tag{30}$$

$$\tilde{x} = \frac{x}{L}, \tag{31}$$

$$\tilde{u} = \frac{u}{u_0}, \tag{32}$$

$$\tilde{t} = \frac{t}{T^*}, \tag{33}$$

$$\tilde{\tau} = \frac{\tau}{\tau_0}, \tag{34}$$

$$\tilde{J^q} = \frac{J^q}{J_0^q}, \tag{35}$$

$$\tilde{T} = \frac{T}{T_0}, \tag{36}$$

$$\tilde{e} = \frac{e}{e_0}, \tag{37}$$

$$\tag{38}$$

where ρ_0 is a reference density, P_0 is a reference pressure, L is a reference length scale, u_0 is a reference velocity, T^* is a reference time scale, τ_0 is a reference stress tensor, J_0^q is a reference heat flux, T_0 is a

reference temperature, and e_0 is a reference internal energy. The relationships between reference values and quantities are:

$$u_0 = \sqrt{\frac{P_0}{\rho_0}}, \tag{39}$$

$$T^* = \frac{L}{u_0}, \tag{40}$$

$$\tau_0 = \frac{4}{3}\frac{\mu u_0}{L}, \tag{41}$$

$$J_0^q = \kappa\frac{T_0}{L} = \frac{\kappa P_0}{RL\rho_0} = \frac{\gamma}{\gamma-1}\frac{\kappa P_0}{c_p L\rho_0}, \tag{42}$$

$$T_0 = \frac{P_0}{\rho_0 R}, \tag{43}$$

$$e_0 = c_v T_0 = \frac{1}{\gamma-1}\frac{P_0}{\rho_0}. \tag{44}$$

The nondimensional groups are

$$Re = \frac{u_0\rho_0 L}{\mu}, \tag{45}$$

$$Pr = \frac{c_p\mu}{\kappa}. \tag{46}$$

The final non-dimensional equations are

$$\frac{\partial\tilde{\rho}}{\partial\tilde{t}} + \frac{\partial}{\partial\tilde{x}}(\tilde{\rho}\tilde{u}) = 0, \tag{47}$$

$$\frac{\partial}{\partial\tilde{t}}(\tilde{\rho}\tilde{u}) + \frac{\partial}{\partial\tilde{x}}\left(\tilde{\rho}\tilde{u}^2 + \tilde{P} - \frac{4}{3}\frac{1}{Re}\tilde{\tau}\right) = 0, \tag{48}$$

$$\frac{\partial}{\partial\tilde{t}}\left(\tilde{\rho}\left(\frac{1}{\gamma-1}\tilde{e} + \frac{\tilde{u}^2}{2}\right)\right) + \frac{\partial}{\partial\tilde{x}}\left(\tilde{\rho}\tilde{u}\left(\frac{1}{\gamma-1}\tilde{e} + \frac{\tilde{u}^2}{2}\right) + \tilde{u}\left(\tilde{P} - \frac{4}{3}\frac{1}{Re}\tilde{\tau}\right) + \frac{\gamma}{\gamma-1}\frac{1}{Re}\frac{1}{Pr}\tilde{J^q}\right) = 0, \tag{49}$$

$$\tilde{\tau} = \frac{\partial\tilde{u}}{\partial\tilde{x}}, \tag{50}$$

$$\tilde{J^q} = -\frac{\partial\tilde{T}}{\partial\tilde{x}}, \tag{51}$$

$$\tilde{P} = \tilde{\rho}\tilde{T}, \tag{52}$$

$$\tilde{e} = \tilde{T}. \tag{53}$$

For the Sod problems $Re = 6526$ and $Pr = 0.7186$. The Shu-Osher problem used the values $Re = 37382$ and $Pr = 0.7186$.